Mo-edge reconstructions in MoSe$_2$ and MoS$_2$: Reexamination of the mechanism

Yinti Ren,[1,2,3] Yijian Hu,[2] Liang Hu,[3] Yuantao Chen,[2] Li Huang ®,[2,*] and Xingqiang Shi ®[1,†]

[1]*Key Laboratory of Optic-Electronic Information and Materials of Hebei Province, Institute of Life Science and Green Development,
College of Physics Science and Technology, Hebei University, Baoding 071002, China*
[2]*Department of Physics, Southern University of Science and Technology, Shenzhen 518055, China*
[3]*Harbin Institute of Technology, Harbin 150080, China*

For zigzag nanoribbons of transition metal dichalcogenides (TMDCs), experiments show a band gap with different gap size at the Mo edges, while theoretical models often predict metallic edges. Such an inconsistency could be attributed to the inadequate understanding of the possible mechanisms of edge reconstructions. Here, we revisit the mechanisms of different edge reconstructions along the Mo edge of MoX$_2$ (X = Se, S) zigzag nanoribbons by first-principles calculations. We demonstrate that the valency of $\frac{1}{3}$ edge Mo increases to 5+ with X adatom reconstruction, or all edge Mo decreases to 3+ with a Mo trimer reconstruction. Based on these Mo valence reconstructions, thermodynamically stable reconstructions are proposed for the Mo edge in 6× and 4× periodicities, which are comparable with the recent experimental observation of a small energy gap (of 0.36 eV) at the Mo edge of zigzag MoSe$_2$ nanoribbons. The edge Mo valency reconstruction leads to quasi-one-dimensional Peierls distortion and charge- and spin-density waves at the edge. These findings should be applicable to other TMDCs.

I. INTRODUCTION

Two-dimensional (2D) transition metal dichalcogenides (TMDCs) have attracted intensive attention because of their unique physical and chemical properties and various applications [1–3]. Semiconducting TMDCs enable a wide tunability of their band gaps, which is essential for applications in electronics [4], optoelectronics [5], spintronics [6], and catalysts [7], etc. However, actual applications often need further reduction of their dimensionality and creation of edges. A variety of edges are often observed, which usually display properties and structure different from their 2D bulk [8–11].

The zigzag and armchair edges are prototypical edges, and the zigzag edges are more stable and observed more often in experiments. There are two distinctly different zigzag edges in TMDCs, the metal-terminated edge and the chalcogen-terminated edge for the ideally bulk truncated forms. The metal edges can adsorb S (or Se) adatoms or other atoms/molecules [12]. Indeed, edge reconstructions [which are one-dimensional (1D) analogues of surface reconstructions] frequently occur. Different edge reconstructions of TMDCs have been shown to be metallic, half-metallic or semiconducting, and ferromagnetic or nonmagnetic [13–16]. Under Mo-rich conditions, the Mo-terminated edges were observed, and two types of reconstructions, distorted 1T (DT) and the Mo-Klein edge, were reported in nanoporous MoS$_2$ films [17]. A MoSe$_2$ nanoribbon with a bottom-up fabrication has a band gap of 0.36 and 0.64 eV at the Mo and Se

edges, respectively [18]. A Mo (or W) trimer reconstruction in the Mo (or W) zigzag edge is proposed theoretically with a (2 × 1) supercell for MoX$_2$ and WX$_2$ (X = S, Se) nanoribbons, in which the Mo (W) edge states exhibit a metallic (half-metallic) behavior with ferromagnetic ordering [19,20]. The driving force of this type of reconstruction is attributed to the Peierls distortion of a quasi-1D atomic chain along the edge. Lucking *et al.* [21] proposed that a (3 × 1) periodicity is necessary to open the band gap at the edge, and the valency increase of $\frac{2}{3}$ of edge Mo atoms increases the band gap size. The charge- and spin-density waves (CDWs/SDWs) are also reported for the MoS$_2$ zigzag edges, although it seems that the CDW/SDW is not compatible with the Mo valency fluctuation [11]. In addition, most previous theoretical works predicted edge reconstructions with a metallic character [18,19,22].

In this paper, by first-principles density function theory calculations, we revisit the possible mechanisms of semiconducting reconstructions along the Mo edge of zigzag MoX$_2$ (X = Se, S) nanoribbons in different reconstruction models. According to the electron counting rule (ECR) [23], a reconstruction with doping $\frac{4}{3}$ holes per edge Mo is needed. However, the Mo edge with this type of reconstruction is metallic, which has been attributed to the valency increase of $\frac{2}{3}$ of Mo edge atoms [21]. To revisit the possible valency fluctuations of edge Mo in different reconstruction models, we use pseudohydrogen (pseudo-H) with electrons between 0.25 and 0.75 to passivate the distinct reconstruction models of Mo edges. We found two Mo valency reconstructions; both can result in semiconducting Mo edges with a small energy gap: (1) the valency of $\frac{1}{3}$ edge Mo atoms increases to 5+ for the S (or Se) adatom reconstruction [21], or (2) all edge Mo valency decreases to 3+ for the Mo trimer reconstruction [18].

---

*huangl@sustech.edu.cn
†shixq20hbu@hbu.edu.cn

Compared with the reported $3\times$ periodicity along the zigzag edge [21], we find a $4\times$ periodicity can also open a band gap. In addition, we show that the valency reconstruction of partial edge Mo atoms is compatible with the appearance of CDW and SDW along the Mo edge.

II. CALCULATION METHODS

Spin-polarized density functional theory calculations were performed using the Vienna *ab initio* Simulation Package (VASP) with periodic boundary conditions [24–26]. The projector augmented wave pseudopotential was adopted to describe the core electrons [27]. The valence electrons were described by plane waves with a cutoff kinetic energy of 350 eV. All calculations were carried out using the Perdew-Burke-Ernzerhof (PBE) form of the generalized gradient approximation density functional [28]. The atomic positions were relaxed until the force on each atom was <0.02 eV Å^{-1} with the Se (or S)-terminated edge fixed. The energy convergence value between two consecutive self-consistent steps was set as 10^{-5} eV. We also consider the onsite Coulomb repulsion of transition metal Mo d orbitals, where the single parameter $U - J$ value is 3 eV [10,29]. The Brillouin zone was sampled in the Monkhorst-Pack scheme with a K-point sampling of $16 \times 1 \times 1$ [for (2×1) supercell] and $4 \times 1 \times 1$ [for (6×1) supercell]. Since a nanoribbon is a 1D system, vacuum regions of 15 Å were added between periodic images of the nanoribbon in the two perpendicular directions. Eight-zigzag chains of nanoribbons were chosen to minimize the interaction between the two edges. Compared with the Mo edge, the chalcogen-terminated edge contains kinks of nanometers in width [30,31], which deserves a separate detailed study in future work. Here, we treat the chalcogen-terminated edge with a simple reconstruction model as that used in the literature [19].

III. RESULTS AND DISCUSSIONS

A. ECR

For a 2D semiconductor, when an edge (analogue to a surface of a three-dimensional bulk) is formed, there exists dangling bonds, which are unstable and need to be stabilized by edge reconstruction. The stability criterion of a structural reconstruction (accompanied with electronic reconstruction) is that all the dangling bonds of the anions (cations) at the edge are occupied (empty) [32]. The ECR is successfully used in group III–V and II–VI compounds [23,33]. For monolayer MoX_2 ($X =$ Se, S) nanoribbons, each Mo has six nearest neighbor X and each X has three nearest neighbor Mo. Each Mo donates four electrons to the six nearest neighbor X, and each X accepts two electrons from the nearest neighbor Mo. Mo donates $\frac{2}{3}$ ($\frac{4}{6} = \frac{2}{3}$) electrons per Mo-$X$ bond. Mo and X in the 2D bulk meet the stability criteria. At the ideal unreconstructed Mo-terminated edge of zigzag MoX_2 ($X =$ Se, S) nanoribbons, the edge Mo has only four nearest neighboring X, and there are two Mo-X bonds broken; the Mo dangling bonds can be passivated by adatoms (Se or S) and/or self-passivated through other reconstruction models to meet the stability criteria. Thus, each (1×1) unreconstructed Mo edge has $\frac{4}{3}$ ($\frac{2}{3} \times 2 = \frac{4}{3}$) electrons. According to the ECR, doping
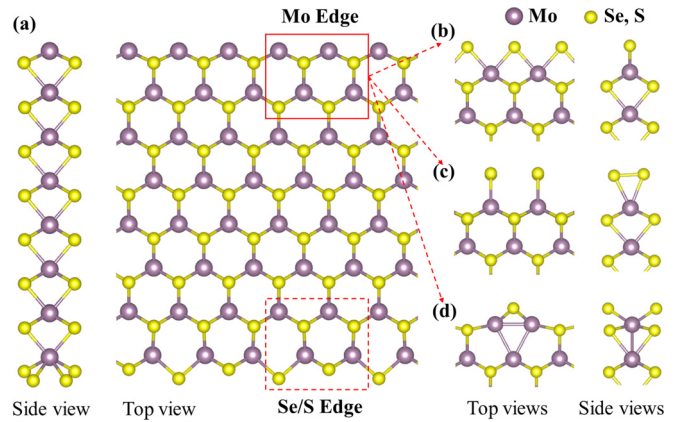

FIG. 1. MoX_2 ($X =$ Se, S) nanoribbons with different reconstructions at the Mo edge. (a) The 8-zigzag MoX_2 nanoribbons with a (2×1) reconstruction at the X-terminated edge; three kinds of literature reported reconstructions at the Mo edge: (b) X-adatom, (c) X-dimer, and (d) Mo-trimer; (b) and (c) with nonstoichiometric ratio, while (d) with the stoichiometric ratio of M:$X = 1 : 2$ along the edge.

$\frac{4}{3}$ holes is needed, such as a (6×1) supercell with four X ($X =$ Se, S) adatoms ($\frac{4}{3} \times 6 = 2 \times 4$). However, this type of reconstruction gives a gapless edge (Fig. S1 in the Supplemental Material [34]); the reconstruction and band structure can be found in the Supplemental Material [34]. That means that we cannot treat this system with the original ECR because the valency of Mo fluctuates at the edge [21]. To know the possible valences of edge Mo in different reconstruction models, we use pseudo-H [35] passivation to study it. The charge of pseudo-H atoms can be fractional (from 0.25 to 0.75 in this paper) and usually used in surface calculations to passivate the dangling bonds to meet ECR.

B. Pristine and reconstructed edges

The optimized lattice constant of a $MoSe_2$ (MoS_2) nanoribbon is 3.307 (3.161) Å, which agrees with the theoretical and experimental results in the literature [36,37]. The geometry structures of MoX_2 ($X =$ Se, S) nanoribbon with a simplified (2×1) reconstruction at the Se (S) edge is adopted [19], so that the supercells in the following are always $(2n \times 1)$, where n is an integer. Three possible reconstructions at the Mo edge are shown in Figs. 1(b)–1(d). Firstly, we consider the pristine edge of $MoSe_2$ with a (2×1) supercell. The band structure of the nanoribbon with the pristine edge shows that there are many states around the Fermi energy; four bands cross the Fermi energy and close the band gap of 2D bulk $MoSe_2$ (Fig. S2(a) in the Supplemental Material [34]). One spin-up band goes up from Γ to X (contributed by the Se edge), and the other three bands come from the Mo edge. As reported in the literature, the pristine Mo edge is metallic and ferromagnetic [38] when the Mo edge adsorbs two Se dimers in a (2×1) supercell [Fig. 1(c)] [22,39]. The band structure (Fig. S2(c) in the Supplemental Material [34]) of the reconstructed Mo edge with the Se dimer is like that of the pristine edge. Then we consider the Mo edge adsorbs Se single atoms, such as a (2×1) supercell with two Se
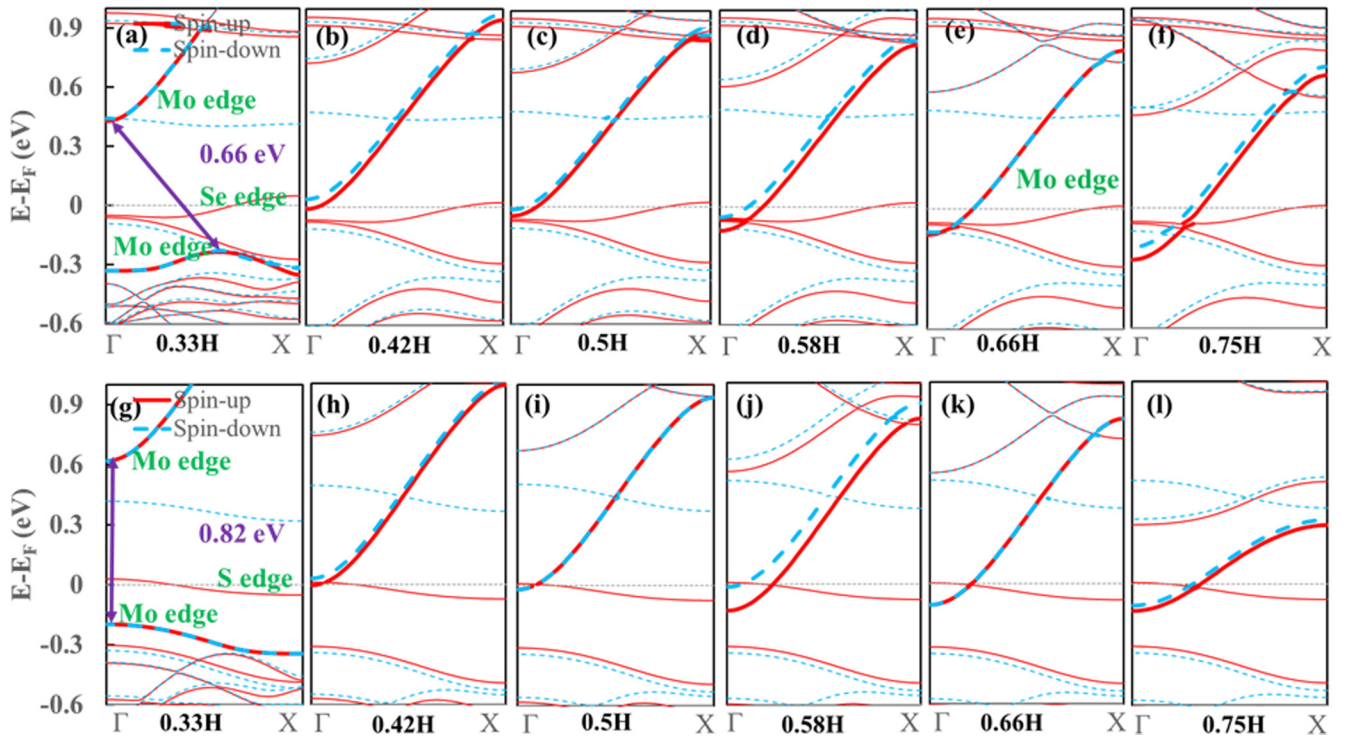
FIG. 2. Band structure evolution of the Mo edge with Se (or S) adatom adsorbing pseudo-H. 0.33H means pseudo-H with 0.33 electrons, and so on. The purple arrows denote the band gap. The upper panels (a)–(f) are for MoSe₂ and that of MoS₂ is in the bottom panels (g)–(l). The Mo and Se (S) edge states are labeled out. The Fermi energy is set to zero.

adatoms [Fig. 1(b)] [22,39]. The band structure shows that the Mo edge is also metallic and ferromagnetic (Fig. S2(b) in the Supplemental Material [34]). However, compared with the pristine edge, there are less states around the Fermi energy, and three bands cross the Fermi energy. This means the weakening of the metallic and ferromagnetic character of the Mo edge, hence the Mo edge with adatoms becomes more stable than the pristine Mo edge and that with the Se dimer. Finally, we consider a Mo trimer reconstruction as proposed in a recent theoretical work [Fig. 1(d)] [19]. We have calculated its band structure (Fig. S2(d) in the Supplemental Material [34]), which shows weakened metallic character and agrees with that in the literature. Compared with the other two kinds of reconstructions in Figs. 1(b) and 1(c), only two bands cross the Fermi energy, one from the Mo edge and another from the Se edge. All the above three types of reconstructions have Mo edge states passing through the Fermi energy and being spin polarized. A small energy gap at the Mo edge has been observed experimentally for MoSe₂ [18], and a mixed edge structure was proposed theoretically to give a small energy gap for MoS₂ [21]. It is necessary to consider a wide range of possible reconstructions to be compatible with experimental results. The mechanism of the semiconducting reconstructions of the Mo edge with a small energy gap needs further investigation.

C. Pseudo-H passivation

Here, we consider the adsorption of pseudo-H to the Se atom at the Mo edge to mimic doping different numbers of holes to the Mo edge, for both the adatom reconstruction

[Fig. 1(b)] and the Mo trimer reconstruction [Fig. 1(d)]. According to the ECR, for the Se adatom reconstruction, the edge Mo atoms donate $\frac{4}{3}$ electrons to each Se adatom, so we need to adsorb pseudo-H with $\frac{2}{3}$ ($2 - \frac{4}{3} = \frac{2}{3}$) electrons on Se adatoms (Fig. S3 in the Supplemental Material [34], two pseudo-H in a (2×1) supercell). The corresponding band structure is shown in Fig. 2(e). This Mo edge is metallic and ferromagnetic. Then we try to dope different electrons to the Se adatoms at the Mo edge, as listed in Figs. 2(a)–2(f). As the doping electrons gradually decrease, we can see that the bands of the Mo edge are gradually raising up while that of the Se edge do not move. When doping pseudo-H with $\frac{1}{3}$ (0.33) electrons, the Mo edge opens an energy gap. In this reconstruction, each Se accepts $\frac{1}{3}$ electrons from the pseudo-H, so accepting $\frac{5}{3}$ ($2 - \frac{1}{3} = \frac{5}{3}$) electrons from Mo. Then each Mo at the Mo edge donates $\frac{13}{3}$ ($\frac{5}{3} + \frac{2}{3} \times 4 = \frac{13}{3}$) electrons to the nearest neighbor Se atoms. Thus, the average valency of Mo is increased to $\frac{13}{3} = 4.33$. Thus, there are actually $\frac{5}{3}$ electrons at the (1×1) pristine Mo edge, different to the original ECR ($\frac{4}{3}$ electrons). The reason for this difference is that there is not only structural reconstruction but also electronic reconstruction, namely, the Mo valency increases (due to edge S adatoms have less Mo neighbors). According to $\frac{5}{3} = 2 \times \frac{5}{6}$ electrons per (1×1) Mo edge, adsorbing five Se adatom in (6×1) supercell could reach the semiconducting edge; here, two denotes two Se (or S) adatoms bonding with the edge Mo. For the Se (or S) element, its valency is 2−. However, for transition metal like Mo, its valency can change from 4+ to 5+ (not 6+) [21] or decrease its valency in a reconstruction with less Se (or S) neighbors.
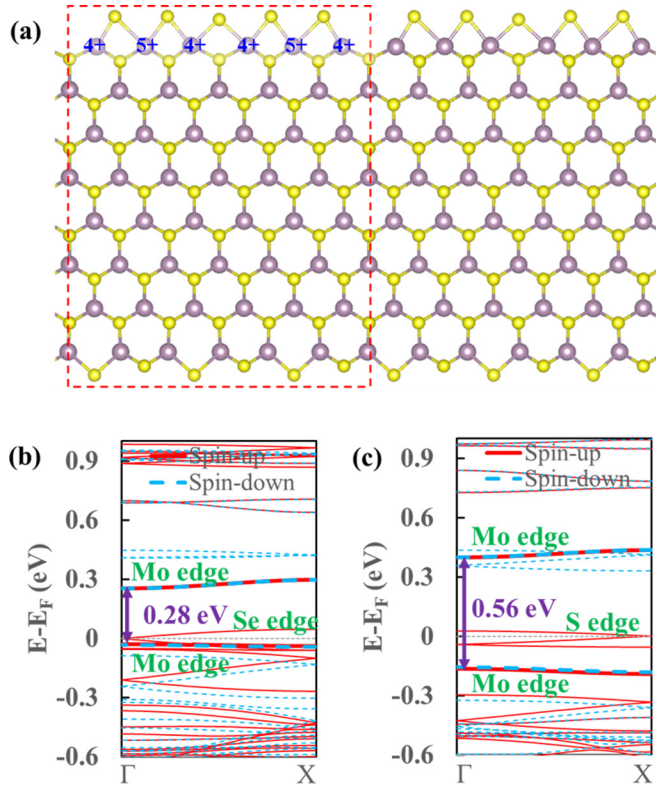
FIG. 3. Small band gap with a reconstruction. (a) The (6×1) reconstruction of Mo edge of $MoSe_2$ (MoS_2) with 5 Se (S) adatoms. The valency of edge Mo is marked. (b) $MoSe_2$ and (c) MoS_2 band structures. Their Mo edge states are below the Fermi energy. The Mo and Se (S) edge states are labeled out. The band gap of Mo edge is marked by purple arrows.

TABLE I. Calculated band gap size of Mo edge in different reconstruction models, and that from literature are given for comparison. The numbers in bracket are from PBE $+ U$ calculations.

Reconstruction models	MoS_2 (eV)	$MoSe_2$ (eV)
Mo trimer (with real hydrogen)	0.27 (0.24)	0.28 (0.28)
5 S/Se adatoms in (6×1) supercell	0.56 (0.92)	0.28 (0.45) 0.36 (Expt.) [18]
6 S/Se adatoms in (6×1) supercell	0.75 0.71 (Theor.) [21] 0.70 (Theor.) [10]	0.60

D. Small band gap with a reconstruction

Figure 3(a) shows the geometric structure of a $MoSe_2$ nanoribbon with five Se adatoms in a (6×1) supercell, and the corresponding band structure is shown in Fig. 3(b). Because the supercell is larger by three times to the (2×1) supercell, the Se edge states at the Fermi energy are folded three times. We can see that the Mo edge states are below the Fermi energy and open a gap of 0.28 eV. Considering the on-site Coulomb repulsion of transition metal Mo d orbitals, the band gap is 0.45 eV (Fig. S4(a) in the Supplemental Material [34]). Our results are also comparable with the recent experimental observation of a small energy gap (0.36 eV) at the Mo edge of zigzag $MoSe_2$ nanoribbons [18], also see Table I. To test our reconstruction model, we also calculated the Mo edge structure with two Mo vacancies and one Se adatom, which also satisfy the edge Mo with an average valency of 4.33+. The corresponding geometric structure and band structure are shown in Figs. S5(a) and S5(b) in the Supplemental Material [34], with an energy gap of 0.15 eV at the Mo edge. Thus, we can propose a semiconducting reconstruction of the Mo edge which satisfies an average Mo valency of 4.33+ for Mo at the edge. For the Mo edge of a MoS_2 nanoribbon, the band gap can be opened by the valency increase of $\frac{2}{3}$ Mo edge atoms from 4+ to 5+, as reported in the literature [21]. Thus, we also calculated with six Se adatoms in the (6×1) reconstruction of the Mo edge of $MoSe_2$. The optimized structure also shows

a $3\times$ periodicity in the Mo edge (Fig. S6(a) in the Supplemental Material [34]), and the Mo edge states have a gap of 0.60 eV (Fig. S6(b) in the Supplemental Material [34]). In this, the Mo average valency is 4.66+ for Mo at the edge. The common valency state of Mo is 4+, and other valency states such as 5+ and 3+ may occur. In the (6×1) reconstruction, if the edge of the Mo average valency is 4.66+, the six Mo of total valency is 28+ $[(\frac{14}{3}+) \times 6 = (28+)]$; it may be that two Mo of valency is 4+ and four Mo of valency is 5+ $[(4+) \times 2 + (5+) \times 4 = (28+)]$ [21]. If the edge of the Mo average valency is 4.33+, the six Mo of total valency is 26+ $[(\frac{13}{3}+) \times 6 = (26+)]$; it may be that two Mo of valency is 5+ and four Mo of valency is 4+ $[(5+) \times 2 + (4+) \times 4 = (26+)]$. To confirm the above proposed Mo valency distribution (of $\frac{1}{3}$ edge Mo atoms), we have replaced four Mo atoms by four Zr atoms (Zr always in valency 4+) in the Mo edge [21]. In our structure, there are three kinds of possible multivalency patterns (considering the $3\times$ periodicity along the Mo edge). The calculated results with testing Zr show that the gap remains only in one multivalency pattern, which indicates that the remaining two Mo atoms are in a valency of 5+ (Fig. S7(a) in the Supplemental Material [34]). The most stable multivalency pattern is shown in Fig. 3(a).

E. Valency fluctuation-induced CDW/SDW

For the (6×1) reconstruction, the Mo valency fluctuation at the edge induces distortion in the quasi-1D geometric structure along the Mo edge. The geometric distortion may lead to the CDW and/or SDW at the edge [10,11], which is confirmed in Fig. 4. There exist a combined CDW/SDW along with structural distortions for both MoS_2 and $MoSe_2$. Note that the valency change of Mo may not be described from Bader charge analysis [10] due to (1) the covalent character of Mo-Se and Mo-S bonds and (2) the charge delocalization in the 2D crystal.

F. Decrease of Mo valency

Similarly, we adsorb pseudo-H in the reconstruction model of Fig. 1(d), as shown in Fig. S8(a) in the Supplemental Material [34]. When adsorbing pseudo-H with 0.25 electrons, the calculation band structure of the Mo edge for both $MoSe_2$ and MoS_2 shows a semiconducting character (Figs. S8(b) and S8(c) in the Supplemental Material [34]). The Mo trimer
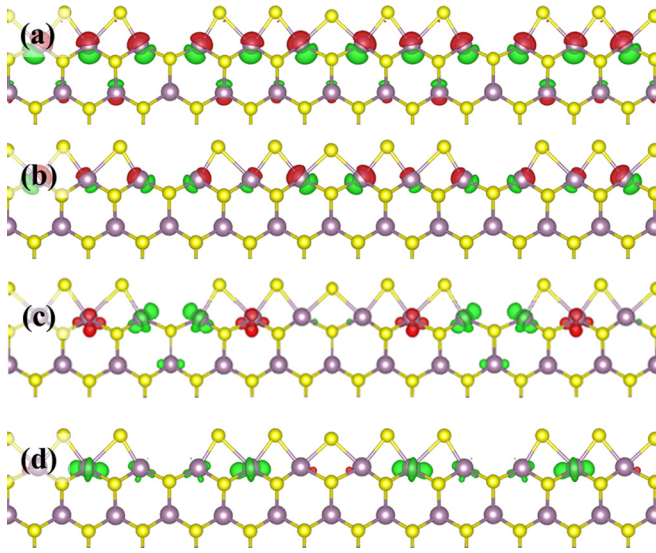
FIG. 4. Charge-density wave (CDW) and spin-density wave (SDW) at the Mo edge in a (6×1) reconstruction with five Se (or S) adatoms. The CDW of (a) $MoSe_2$ and (b) MoS_2. The SDW of (c) $MoSe_2$ and (d) MoS_2. The red/green colors indicate the change in charge density for CDW, ($\Delta\rho = \rho_{relaxed} - \rho_{unrelaxed}$) between relaxed and unrelaxed structures. For SDW, the red/green colors indicate the density of spin up/down wave functions.

donates $\frac{7}{2}$ (two pseudo-H donate $\frac{1}{2}$ electrons) electrons to outside Se (two Se atoms above each Mo trimer) and donates $\frac{16}{3}$ ($\frac{2}{3} \times 8 = \frac{16}{3}$) electrons to inside Se (eight Se atoms around each Mo trimer) since the total valency of the Mo trimer is 8.83+, and average valency of Mo is ~3+. In experiment, hydrogen, oxygen, and other atoms may adsorb on the edge. Here, we adsorb one hydrogen atom per (4×1) supercell [Fig. 5(a)]; the band gap remains. The Mo edges of $MoSe_2$ and MoS_2 have gaps of 0.28 and 0.27 eV in the PBE level [Figs. 5(b) and 5(c)] and 0.28 and 0.24 eV in the PBE + U level (Fig. S9 in the Supplemental Material [34]), respectively. Thus, a semiconducting reconstruction can also be obtained by decreasing the Mo valency at the edge. In addition to the $3\times$ periodicity proposed in the literature [21], $4\times$ periodicity can open a band gap along the zigzag edge.

G. Molybdenum disulfide

We apply the same Mo valency change ($\frac{1}{3}$ edge Mo increase to 5+ or all edge Mo decrease to 3+) to probe the semiconducting reconstructions of the Mo edge of a MoS_2 zigzag nanoribbon. Firstly, we calculate three structures like that in Figs. 1(b)–1(d), namely, adsorbing two S adatoms, two S dimers, and a Mo trimer in the (2×1) reconstruction. The results are shown in Figs. S2(f)–S2(h) in the Supplemental Material [34]. All of them are also metallic and ferromagnetic. The S edge state always has one band across the Fermi energy. Then we take pseudo-H passivation to study the Mo edge with two S adatoms in a (2×1) reconstruction (Fig. S3 in the Supplemental Material [34]). The pseudo-H charge is equal to that in $MoSe_2$. The band structures [Figs. 2(g)–2(l)] show that pseudo-H with $\frac{1}{3}$ electrons can open a gap (0.82 eV) at the Mo edge. In the (6×1) reconstruction, adsorbing five S
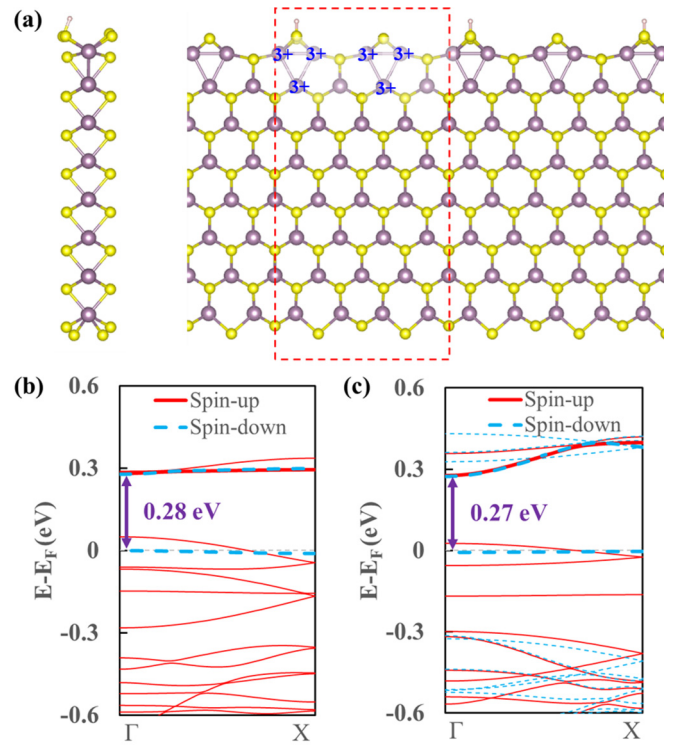

FIG. 5. Band gap opening with a $4\times$ periodicity along the zigzag edge. (a) One hydrogen atom in a (4×1) reconstruction with Mo trimers. The valency of edge Mo is marked. (b) $MoSe_2$ and (c) MoS_2 band structures. Their Mo edge states are below the Fermi energy. The band gap at Mo edge is marked by purple arrows.

adatoms at the Mo edge has a gap of 0.56 eV [Fig. 3(c)] and 0.92 eV (PBE + U; Fig. S4(b) in the Supplemental Material [34]), and adsorbing six S adatom at the Mo edge has a gap of 0.75 eV (Fig. S6(c) in the Supplemental Material [34]), which agree with the theoretical results in the literature (Table I) [21]. Different gap sizes appear for 6 vs 5 S adatoms in the (6×1) reconstructions due to (1) the Mo edges are different (6 vs 5 S adatoms) and (2) the valence reconstructions of the edge Mo are different (the valency of $\frac{2}{3}$ vs $\frac{1}{3}$ Mo increase to 5+). When the Mo edge has two Mo vacancies and one S adatom, the Mo edge can also have a gap (0.07 eV), as shown in Fig. S5(d) in the Supplemental Material [34].

IV. CONCLUSIONS

The mechanism for different types of reconstructions along the Mo edge are revisited, and we propose that the valency reconstruction is compatible with the resulted CDW and SDW along the Mo edge. The Mo edges with a smaller energy gap can be obtained by both valency increase and valency decrease of edge Mo atoms. A $4\times$ periodicity can also open a band gap along the Mo edge. In addition to the mixed edge structures proposed in the literature [21], the Mo edge with five Se adatoms in a (6×1) supercell has a small band gap at the Mo edge [0.28 eV (PBE), 0.45 eV (PBE + U)] and, with a Mo trimer reconstruction (with hydrogen atom adsorption), has an energy gap of 0.28 eV for both PBE and PBE + U, which are also in agreement with the scanning tunneling microscopy

measured gap of 0.36 eV. The findings in this paper should be applicable to other TMDCs.

ACKNOWLEDGMENTS

[1] M. Chhowalla, H. S. Shin, G. Eda, L. J. Li, K. P. Loh, and H. Zhang, The chemistry of two-dimensional layered transition metal dichalcogenide nanosheets, Nat. Chem. **5**, 263 (2013).

[2] Y. Zhang, Y. Zhang, Q. Ji, J. Ju, H. Yuan, J. Shi, T. Gao, D. Ma, M. Liu, Y. Chen, X. Song, H. Y. Hwang, Y. Cui, and Z. Liu, Controlled growth of high-quality monolayer WS_2 layers on sapphire and imaging its grain boundary, ACS Nano **7**, 8963 (2013).

[3] S. Tongay, W. Fan, J. Kang, J. Park, U. Koldemir, J. Suh, D. S. Narang, K. Liu, J. Ji, J. Li, R. Sinclair, and J. Wu, Tuning interlayer coupling in large-area heterostructures with CVD-Grown MoS_2 and WS_2 monolayers, Nano Lett. **14**, 3185 (2014).

[4] Q. H. Wang, K. Kalantar-Zadeh, A. Kis, J. N. Coleman, and M. S. Strano, Electronics and optoelectronics of two-dimensional transition metal dichalcogenides, Nat. Nanotechnol. **7**, 699 (2012).

[5] G. H. Shin, C. Park, K. J. Lee, H. J. Jin, and S.-Y. Choi, Ultrasensitive phototransistor based on WSe_2-MoS_2 van der Waals Heterojunction, Nano Lett. **20**, 5741 (2020).

[6] D. Xiao, G. B. Liu, W. Feng, X. Xu, and W. Yao, Coupled Spin and Valley Physics in Monolayers of MoS_2 and Other Group-VI Dichalcogenides, Phys. Rev. Lett. **108**, 196802 (2012).

[7] A. Azizi, M. Dogan, H. Long, J. D. Cain, K. Lee, R. Eskandari, A. Varieschi, E. C. Glazer, M. L. Cohen, and A. Zettl, High-performance atomically-thin room-temperature NO_2 Sensor, Nano Lett. **20**, 6120 (2020).

[8] R. Rani, A. Yoshimura, S. Das, M. R. Sahoo, A. Kundu, K. K. Sahu, V. Meunier, S. K. Nayak, N. Koratkar, and K. S. Hazra, Sculpting artificial edges in monolayer MoS_2 for controlled formation of surface-enhanced Raman hotspots, ACS Nano **14**, 6258 (2020).

[9] K. Chen, J. Deng, X. Ding, J. Sun, S. Yang, and J. Z. Liu, Ferromagnetism of 1T′-MoS_2 nanoribbons stabilized by edge reconstruction and its periodic variation on nanoribbons width, J. Am. Chem. Soc. **140**, 16206 (2018).

[10] S. Krishnamurthi, M. Farmanbar, and G. Brocks, One-dimensional electronic instabilities at the edges of MoS_2, Phys. Rev. B **102**, 165142 (2020).

[11] S. Krishnamurthi and G. Brocks, Spin/charge density waves at the boundaries of transition metal dichalcogenides, Phys. Rev. B **102**, 161106(R) (2020).

[12] T. Chowdhury, E. C. Sadler, and T. J. Kempa, Progress and prospects in transition-metal dichalcogenide research beyond 2D, Chem. Rev. **120**, 12563 (2020).

[13] Y. Li, Z. Zhou, S. Zhang, and Z. Chen, MoS_2 nanoribbons: high stability and unusual electronic and magnetic properties, J. Am. Chem. Soc. **130**, 16739 (2008).

[14] X. Deng, Z. Li, and J. Yang, One-dimensional magnetic order stabilized in edge-reconstructed MoS_2 nanoribbon via bias voltage, J. Phys. Chem. Lett. **11**, 7531 (2020).

[15] A. Pulkin and O. V. Yazyev, Controlling the quantum spin hall edge states in two-dimensional transition metal dichalcogenides, J. Phys. Chem. Lett. **11**, 6964 (2020).

[16] R. Xu, B. Liu, X. Zou, and H.-M. Cheng, Half-metallicity in Co-doped WSe_2 nanoribbons, ACS Appl. Mater. Interfaces **9**, 38796 (2017).

[17] X. Zhao, D. Fu, Z. Ding, Y.-Y. Zhang, D. Wan, S. J. R. Tan, Z. Chen, K. Leng, J. Dan, W. Fu, D. Geng, P. Song, Y. Du, T. Venkatesan, S. T. Pantelides, S. J. Pennycook, W. Zhou, and K. P. Loh, Mo-terminated edge reconstructions in nanoporous molybdenum disulfide film, Nano Lett. **18**, 482 (2018).

[18] Y. Chen, P. Cui, X. Ren, C. Zhang, C. Jin, Z. Zhang, and C.-K. Shih, Fabrication of $MoSe_2$ nanoribbons via an unusual morphological phase transition, Nat. Commun. **8**, 15135 (2017).

[19] P. Cui, J.-H. Choi, W. Chen, J. Zeng, C.-K. Shih, Z. Li, and Z. Zhang, Contrasting structural reconstructions, electronic properties, and magnetic orderings along different edges of zigzag transition metal dichalcogenide nanoribbons, Nano Lett. **17**, 1097 (2017).

[20] P. Cui, J. Zeng, H. Peng, J.-H. Choi, Z. Li, C. Zeng, C.-K. Shih, J. P. Perdew, and Z. Zhang, Predictive design of intrinsic half-metallicity in zigzag tungsten dichalcogenide nanoribbons, Phys. Rev. B **100**, 195304 (2019).

[21] M. C. Lucking, J. Bang, H. Terrones, Y.-Y. Sun, and S. Zhang, Multivalency-induced band gap opening at MoS_2 Edges, Chem. Mater. **27**, 3326 (2015).

[22] D. Davelou, G. Kopidakis, E. Kaxiras, and I. N. Remediakis, Nanoribbon edges of transition-metal dichalcogenides: stability and electronic properties, Phys. Rev. B **96**, 165436 (2017).

[23] M. D. Pashley, Electron counting model and its application to island structures on molecular-beam epitaxy grown GaAs(001) and ZnSe(001), Phys. Rev. B **40**, 10481 (1989).

[24] G. Kresse and J. Hafner, *Ab initio* molecular dynamics for liquid metals, Phys. Rev. B **47**, 558 (1993).

[25] P. E. Blöchl, Projector augmented-wave method, Phys. Rev. B **50**, 17953 (1994).

[26] G. Kresse and J. Furthmüller, Efficient iterative schemes for *ab initio* total-energy calculations using a plane-wave basis set, Phys. Rev. B **54**, 11169 (1996).

[27] G. Kresse and D. Joubert, From ultrasoft pseudopotentials to the projector augmented-wave method, Phys. Rev. B **59**, 1758 (1999).

[28] J. P. Perdew, K. Burke, and M. Ernzerhof, Generalized Gradient Approximation Made Simple, Phys. Rev. Lett. **77**, 3865 (1996).

[29] S. L. Dudarev, G. A. Botton, S. Y. Savrasov, C. J. Humphreys, and A. P. Sutton, Electron-energy-loss spectra and the structural stability of nickel oxide: an LSDA + U study, Phys. Rev. B **57**, 1505 (1998).

[30] Q. Chen, H. Li, W. Xu, S. Wang, H. Sawada, C. S. Allen, A. I. Kirkland, J. C. Grossman, and J. H. Warner, Atomically flat zigzag edges in monolayer MoS$_2$ by thermal annealing, Nano Lett. **17**, 5502 (2017).

[31] Q. Deng, Q. H. Thi, J. Zhao, S. J. Yun, H. Kim, G. Chen, and T. H. Ly, Impact of polar edge terminations of the transition metal dichalcogenide monolayers during vapor growth, J. Phys. Chem. C **122**, 3575 (2018).

[32] S. C. Rasmussen, The 18-electron rule and electron counting in transition metal compounds: theory and application, ChemTexts **1**, 10 (2015).

[33] W.-J. Lee and Y.-S. Kim, Dimer-vacancy reconstructions of the GaN and ZnO(10-11) surfaces: density functional theory calculations, Phys. Rev. B **84**, 115318 (2011).

[34] See Supplemental Material at http://link.aps.org/supplemental/ 10.1103/PhysRevB.104.115406 for different reconstructions and band structures and Figs. S1–S9.

[35] H.-X. Deng, S.-S. Li, J. Li, and S.-H. Wei, Effect of hydrogen passivation on the electronic structure of ionic semiconductor nanostructures, Phys. Rev. B **85**, 195328 (2012).

[36] Q. Wang, Y. Shao, and X. Shi, Mechanism of charge redistribution at the metal-semiconductor and semiconductor-semiconductor interfaces of metal-bilayer MoS$_2$ junctions, J. Chem. Phys. **152**, 244701 (2020).

[37] X. Guan, G. Zhu, X. Wei, and J. Cao, Tuning the electronic properties of monolayer MoS$_2$, MoSe$_2$ and MoSSe by applying z-axial strain, Chem. Phys. Lett. **730**, 191 (2019).

[38] C. Ataca, H. Şahin, E. Aktürk, and S. Ciraci, Mechanical and electronic properties of MoS$_2$ nanoribbons and their defects, J. Phys. Chem. C **115**, 3934 (2011).

[39] G. Hu, V. Fung, X. Sang, R. R. Unocic, and P. Ganesh, Predicting synthesizable multi-functional edge reconstructions in two-dimensional transition metal dichalcogenides, NPJ Comput. Mater. **6**, 44 (2020).